Water Research 173 (2020) 115569

Contents lists available at ScienceDirect

Water Research

journal homepage: www.elsevier.com/locate/watres

Oil-mineral flocculation and settling velocity in saline water

Leiping Ye [a, *], Andrew J. Manning [a, b, c], Tian-Jian Hsu [a]

[a] Center for Applied Coastal Research, Department of Civil and Environmental Engineering, University of Delaware, Newark, DE, 19716, United States
[b] HR Wallingford Ltd., Coasts and Ocean Group, Wallingford, OX10 8BA, United Kingdom
[c] School of Biological and Marine Sciences, University of Plymouth, Plymouth, PL4 8AA, United Kingdom

ARTICLE INFO

Article history:
Received 30 October 2019
Received in revised form
28 January 2020
Accepted 29 January 2020
Available online 3 February 2020

Keywords:
Oil-mineral aggregates (OMAs)
Flocculation
Settling velocity
Microfloc
Macrofloc

ABSTRACT

Cohesive particles in aquatic systems can play an important role in determining the fate of spilled oil via the generation of Oil-Mineral Aggregates (OMAs). Series of laboratory experiments have been conducted aiming at filling the knowledge gap regarding how cohesive clay particles influence the accumulation of petroleum through forming different aggregate structures and their resulting settling velocity. OMAs have been successfully created in a stirring jar with artificial sea-water, crude oil and two types of most common cohesive minerals, Kaolinite and Bentonite clay. With the magnetic stirrer adjusted to 490 rpm to provide a high level homogeneous flow turbulence (Turbulence dissipation ε estimated to be about 0.02 $m^2 \cdot s^{-3}$), droplet OMAs and flake/solid OMAs were obtained in oil-Kaolinite sample and oil-Bentonite sample, respectively. Kaolinite clay with relatively low flocculation rate ($R_f = 0.13$ min^{-1}) tends to physically attach around the surface of oil droplets. With the lower density of oil, these oil-Kaolinite droplet OMAs generally show lower settling velocity comparing to pure mineral Kaolinite flocs. Differently, Bentonite clay with higher flocculation rate ($R_f = 0.66$ min^{-1}) produces more porous flocs that can absorb or be absorbed by the oil and form compact flake/solid OMAs with higher density and settling velocity than pure Bentonite flocs. In the mixed Kaolinite-Bentonite sample (1:1 in weight), oil is observed to preferably interacting with Bentonite and increase settling velocity especially in larger floc size classes.

1. Introduction

Since the petroleum exploration and transportation became one of the most critical industrial activities for the global economic growth, extremely large oil spill disasters, such as the 1989 Exxon Valdez spill (Peterson et al., 2003) and the 2010 Deepwater Horizon (DWH) disaster (Crone and Tolstoy, 2010; Atlas and Hazen, 2011), and increasingly smaller size spills (Hayakawa et al., 2006; Doshi et al., 2018; Liu and Callies, 2019), had occurred in the coastal zones. These oil spill accidents pose detrimental impacts on sea-based human activities (Peterson et al., 2003) and contamination of aquatic bio-communities (Ainsworth et al., 2018) such as fishes (Murawski et al., 2014), birds (Henkel et al., 2012), coral (White et al., 2012) or plankton (Almeda et al., 2013, 2016). Although most mitigation methods focus on spilt oil floating onto the water surface (Reddy et al., 2002, 2012; Liu et al., 2012), there can be a considerable portion of spilt oil settles to the sea-floor due to flocculation with natural cohesive materials, including sediments and organic particles (Chanton et al., 2014; Yan et al., 2016; Jones and Bridgeman, 2016; Romero et al., 2017; O'Laughlin et al., 2017).

Flocculation with cohesive mineral sediments can be especially common in more energetic coastal environments where resuspension of sediment is more likely or near river mouths where new supplies of sediments are abundant (Strom and Keyvani, 2016; Shen et al., 2018). When crude oil is released into aquatic systems, oil droplets can flocculate with suspended particles (Sterling et al., 2005). Through settling and deposition, the oil mineral aggregates may eventually arrive sea-floor and affects benthic ecosystem (Romero et al., 2017). Therefore, the interactions of oil and aquatic mineral particles, or biological materials can play an important role in the fate of spilt oil (Khelifa et al., 2002, 2005a; Passow and Hetland, 2016; O'Laughlin et al., 2017). This study focuses on the influence of mineral sediments on oil droplets through flocculation. Insights into flocculation of oil droplets with biological materials (e.g., marine snows) can be found in Passow et al. (2012) and a comprehensive review article of Daly et al. (2016).

Oil droplets tend to flocculate with, and be stabilized by,

* Corresponding author.
E-mail address: lye@udel.edu (L. Ye).

https://doi.org/10.1016/j.watres.2020.115569
0043-1354/

cohesive particles or suspended particle materials (SPM) in the water column and form oil-mineral aggregates (OMAs) (Khelifa et al., 2002), oil-SPM aggregates (OSAs) (Khelifa et al., 2005a) or oil-particle aggregates (OPAs) (e.g., Zhao et al., 2014, 2016, 2017). In the present study, the term "OMAs" has been used because only mineral clay was used to flocculate with oil droplets. Several earlier studies focus on the structure of OMAs using microscopy imagery and "droplet OMAs", "flake OMAs" or "solid OMAs" are most commonly observed OMA structures (Lee and Stoffyn-Egli, 2001; Stoffyn-Egli and Lee, 2002). Droplet OMAs are combination or enclosure of one or several oil droplet(s) and mineral particles/flocs via surface attachments. On the contrary, flake OMAs and solid OMAs both have similar membrane-like sheets with an orderly arranged oil and mineral particle configuration (Stoffyn-Egli and Lee, 2002). With higher shear strength, structures of flake OMAs could be altered to become solid OMAs because the crumpling or breaking of flake type OMAs may form more compact and denser floc structures (Stoffyn-Egli and Lee, 2002; Loh et al., 2014).

More quantitative studies of OMAs can be found in, for example, Omotoso et al. (2002), who presented a quantitatively study on flocculation index based on the sedimentation rate of a sheared oil-mineral-water mixture. The degree of interaction of oil and minerals in water was found to be dependent on the viscosity of the crude oil and the type of mineral present. Moreover, Khelifa et al. (2002) reported that the concentration of oil droplets contained in OMA depended on oil viscosity, temperature and asphaltenes-resins content (ARC). Le Floch et al. (2002) quantified the amount of oil incorporated into OMA with the salinity ranging from 0∼35 ppt. They demonstrated that the OMA formation was significantly enhanced by salinity when comparing to distilled water condition. However, the amount of oil contained in OMAs saturated at low salinity of only 2 ppt and further enhancing salinity showed almost no effect on OMA formation. Hill et al. (2002) presented an equation that defines the time required to coat and stabilize oil droplets with mineral particles suspended in a turbulent medium.

With the high demand of quantitative understanding on the formation of OMAs, some further laboratory studies have been reported. Sun et al. (2010, 2013) showed that the formation of OMAs increased exponentially with the mixing time and reached an equilibrium within 4∼5 hrs at a provided turbulence dissipation rate of 2.6 $m^2 \cdot s^{-3}$. They suggested that the shaking rate (turbulence) largely influenced the maximum oil trapping efficiency in OMAs. In low mixing energy condition, most of the aggregates they obtained were solid aggregates and single droplet aggregates, while multi-droplet oil suspended particles aggregates are observed in high mixing energies.

Among all the existing OMA literature, very limited studies have been reported to systematically investigate OMAs settling velocities. Khelifa et al. (2008) reported a series of laboratory jar tests on OMA formation by chemically dispersed oil and natural cohesive sediments. Their data, probably for the first time, showed a direct relationships between the measured settling velocity and OMA size. They suggested that those flocs with low oil concentration may barely change the OMA characteristics, but with high oil concentration within the OMAs, their density can be significantly lower than pure sediment flocs. For most sediment types they tested, the effective density of the oil-sediment aggregates can be about 2∼3 times less than those of pure sediment flocs. Importantly, they also suggested that the presence of chemically dispersed oil may enhance the stickiness of sediment grains which helps building up the large flocs with oil participation. More recently, O'Laughlin et al. (2017) reported measured settling velocity of dilbit-derived OMAs from series of jar tests and wave flume experiments in response to the presence or absence chemical dispersants. They suggested that settling velocities of artificially formed OMAs on the order of 0.1∼0.4 $mm \cdot s^{-1}$. Moreover, the OMA size, settling velocity and effective particle density were increased in response to the higher concentration of suspended sediment. However, their data showed evidences that dispersant may inhibits flocculation. These two studies clearly indicated the importance of cohesion (stickiness) in determining the resulting oil-floc and their settling velocity.

The present study is motivated to investigate the effect of mineral types in determining the OMA structures and the resulting settling velocities. We hypothesize that a main factor controlling the structures of OMA is the stickiness of the mineral sediments, which further leads to different settling characteristics. Data obtained from the controlled laboratory experiments are analyzed with three main objectives: 1) To understand the OMAs structures formed with different types of common clay minerals by high-resolution digital microscopy, 2) to measure physical characteristics of OMAs, such as their sizes and settling velocities using LabSFLOC-2 camera, and to 3) synthesize measured data to gain insights into OMA structure and settling dynamics due to different clay types. The remaining of this paper is organized as follow. Section 2 focuses on the laboratory methods. Measured results are presented in Section 3. Discussions are given in Section 4 and main concluding remarks are provided in Section 5.

2. Materials and methods

2.1. Laboratory experiment setup

An experimental stand set (Fig. 1a) was designed and a series of magnetic stirring jar experiments have been conducted at the Center for Applied Coastal Research, University of Delaware. White Kaolin clay (92.3±2.5 % Kaolinite), Wyoming sodium Bentonite clay (85.2±2.3 % Montmorillonite) and raw Texas crude oil (Dynamic viscosity: 7.27×10^{-3} Pa•s at 20 °C) with various proportions are used to generate OMAs. These two common clay types are chosen due to their large difference in cohesion in saline water. As summarized in Table 1, we specify oil-to-sediment ratio close to 2 with clay mineral concentration of 0.5 g per litre of saline water, which provides a condition for maximum OMA formation efficiency according to the previous studies (Guyomarch et al., 2002; Khelifa et al., 2008; Ajijolaiya et al., 2006). Artificial seawater (Salinity ≈ 35 ppt) has been made from mixing clean water and pure salt. The jar has a diameter of 11 cm and the flow depth is 13 cm (1 L salt water). Magnetic stirring speed is set to 490 rpm (Device range: 0∼1000 rpm) for providing a constant turbulence intensity for OMAs generation. Three-component flow velocities are measured by a Vectrino Profiler (Nortek), which was mounted on the shelf above the magnetic stirrer with the sensor probes located 5 cm below the water surface in the jar (in Fig. 1a). Flow velocity data was collected without crude oil and sediment but in otherwise the same flow conditions. The time series of turbulent velocity fluctuations are transformed into Fourier space to obtain turbulent kinetic energy spectrum. Turbulence dissipation rate is then estimated to be $\varepsilon \approx 0.02\ m^2 \cdot s^{-3}$ via matching the Kolmogorov spectrum with Taylor frozen turbulence approximation (e.g., Voulgaris and Trowbridge, 1998; Huang et al., 2018). All the experiments reported here were carried out in artificial seawater of salinity ≈ 35 ppt at 20 °C with viscosity ≈ 1.08×10^{-3} Pa•s.

Different types of mineral flocs and Oil-Mineral Aggregates (OMAs) samples are generated (see Table 1). Each experimental run last up to 2 hrs and OMAs are allowed to settle down overnight (∼8 hrs) before they are collected for settling column experiment using LabSFLOC-2 system (see next).

The mass settling velocity of OMAs were observed using the

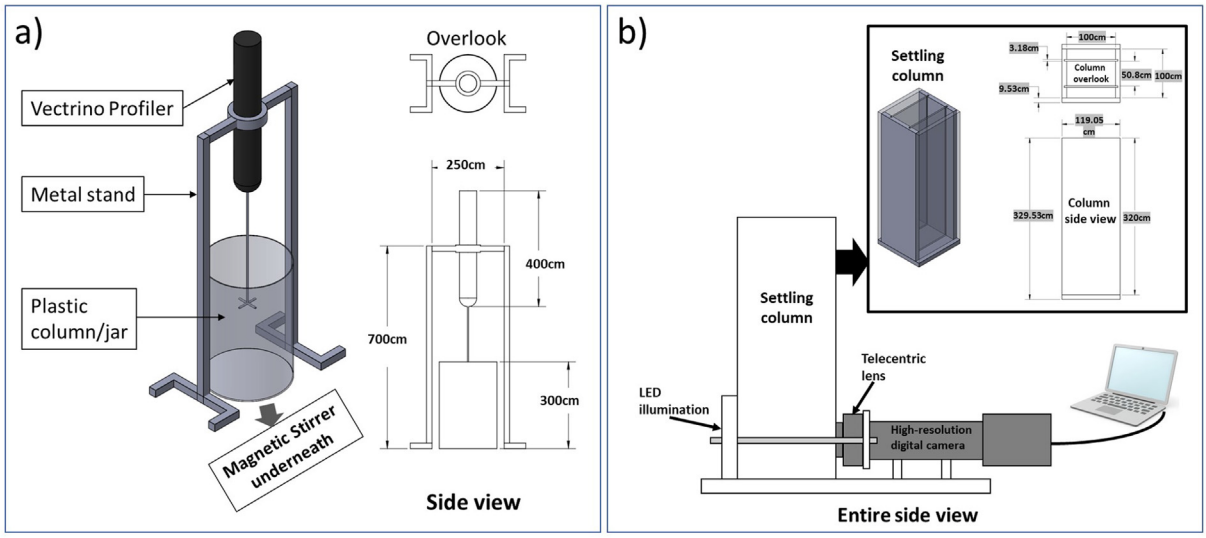

Fig. 1. Schematic of the laboratory experimental setup. Panel a) shows the self-designed Vectrino stand set and panel b) show the LabSFLOC-2 system.

Table 1
A summary on proportions of mineral clay and oil in each experimental run.

Sample	Saline water(L)	Kaolinite clay(g)	Bentonite clay(g)	Texas crude oil(g)
S01	1.00	0.50	/	/
S02	1.00	0.50	/	1.00
S03	1.00	/	0.50	/
S04	1.00	/	0.50	1.00
S05	1.00	0.25	0.25	/
S06	1.00	0.25	0.25	1.00

low intrusive LabSFLOC-2 system (the 2nd version of Laboratory Spectral Flocculation Characteristics instrument) (Fig. 1b). More information on its design and capability can be found in Manning and Dyer (2007) and Gratiot and Manning (2004). The system measures the entire floc population for each sample being assessed and has been successfully applied in many cohesive sediment transport studies (Manning et al., 2010; Manning and Schoellhamer, 2013; Uncles and Mitchell, 2017). LabSFLOC-2 utilizes a low-intrusive 2.0 MP Grasshopper monochrome digital video camera to optically observe individual flocs as they settle in a 350 mm high by 100 mm square Perspex settling column. The video camera, positioned nominally 75 mm above the base of the column, views all particles in the center of the column that pass within a 1 mm depth of field, 45 mm from the Sill TZM 1560 high-magnification (5 μm pixel resolution) Telecentric (maximum pixel distortion of 0.6 %), 0.66 (1:1.5) magnification, F4, macro lens fitted behind a 5 mm thick glass faceplate. The LabSFLOC-2 settling column sampling was conducted at the end of each 2-h floc generation experiment and these OMA samples are in an equilibrium stage.

A high-resolution digital microscope system has been used to observe detailed floc structures and to carry out statistical analysis on floc numbers at different time during the floc generation in order to evaluate flocculation rate. All the floc samples were directly collected from the running experiment in real-time using wide mouth (> 2 mm) plastic pipettes to minimize floc disturbance and to transfer the samples from the mixing jar to the microscope slides without using coverslip to prevent the samples being squeezed. Floc samples are observed with a 4∼10 times zoom-in screen on a DELL laptop by the camera software provided by AmScope Inc.

2.2. Data processing

2.2.1. LabSFLOC-2 camera floc data

The LabSFLOC-2 system produces visible floc individual images that are analyzed to obtain other essential quantitative floc properties including floc size, floc shape and floc settling velocity (Manning et al., 2010). Through additional theories, other floc quantities can be derived, such as floc density, fractal dimension and so on. The recorded videos of floc settling videos can be analyzed with Matlab software routines based on the HR Wallingford Ltd DigiFloc software (Benson and Manning, 2013) and Java Script to semi-automatically process the digital recording image stack to obtain floc size and settling velocity spectra (Manning et al., 2010; Uncles and Mitchell, 2017). Using the measured floc diameter D, settling velocity W_s, and floc shape, a modified Stokes Law (Stokes, 1851) is used to estimate individual floc effective density (Manning and Schoellhamer, 2013):

$$\rho_e = \frac{18 W_s \rho \nu}{g D^2} f(Re) \tag{1}$$

in which ρ the is the saltwater density, ν is the kinematic viscosity, and g is gravitational acceleration. To account for the floc shape effect, the diameters associated with the major and minor axes are identified and the sphere-equivalent diameter is used to calculate floc diameter $D = (D_{major} \cdot D_{minor})^{0.5}$. The Oseen (1927) correction factor is written as $f(Re) = 1/(1 + 0.1875 * Re)$, which accounts for higher particle Reynolds number effect. The particle Reynolds number Re is defined as:

$$Re = \frac{\rho_e W_s D}{\rho \nu} \tag{2}$$

When *Re* is much smaller than unity, the modified Stokes' law shown in Eq. (1) reduces to commonly used Stokes' law. By assuming floc has a fractal structure, the fractal dimension of floc (n_f) can be calculated via the following relationship (Winterwerp and Van Kesteren, 2004):

$$\left(\frac{D}{d}\right)^{n_f-3} = \frac{\rho_e}{\rho_s - \rho} \tag{3}$$

in which $d = 4\ \mu$m is the minimum primary particle size.

2.2.2. Microscope images analysis

The floc images (e.g., Fig. 2a) collected from the digital microscope of each floc sample allow a detailed examination of floc and OMA structures. Microscope images also provide independent and high-resolution data of floc population, which are number counted manually according to the contours, and shape analyzed for further statistical analysis and flocculation rate evaluation. For each sample, six different microscopy images have been analyzed which cover hundreds to thousands individual flocs.

We also use microscope images to estimate averaged oil droplets size under the given turbulence level (e.g., see Fig. 2b). In the inset of Fig. 2b, we present the pure oil droplets size distribution under the given constant turbulence. The statistical analysis of the pure oil droplets samples images shows the maximum oil droplets size can be up to 120 μm and the mean droplets size is approximately 57 μm.

2.2.3. Mineral stickiness quantification via flocculation rate (R_f)

As mentioned before, we expect mineral stickiness plays a key role in determining the corresponding OMA characteristics. In the study of flocculation with significant organic content, such as due to the presence of transparent exopolymer particles (TEP) (e.g., Passow (2002)), the stickiness of each sample was quantified by performing experiments to estimate flocculation (efficiency) rate (Engel, 2000). Similar flocculation rate experiments were carried out in this study for three types of mineral particles without the presence of oil, i.e., cases S01 (Kaolinite), S03 (Bentonite) and S05 (Kaolinite-Bentonite mixture) (see Table 1), respectively. Temporal microscopy images (six images for each sample at a time) have been collected during mineral flocs development in a magnetic stirrer jar from beginning (0 min) to the end (2 h) for each mineral sample. By counting the floc numbers at different instants and normalizing them by the initial floc number of each mineral sample, flocculation evolution time series were obtained for each type of mineral clay (Fig. 3). The manually counted floc numbers cover hundreds to thousands individual flocs which are statistically significant to represent the characteristics of each sample.

Due to flocculation, the number of particles in each case decayed in time. In the semi-logarithmic plot shown in Fig. 3, we observed a nearly exponential decay of particle number in the first couple of minutes of the flocculation before the particle number becomes more or less constant in time. By fitting the first three data points in each run, we obtain the representative flocculation rate: R_f. The three trend lines in Fig. 3 indicate that Kaolinite clay has the lowest flocculation rate of $R_{f\_Kaolinite} = 0.13\ (\text{min}^{-1})$ while the Bentonite clay shows a nearly 5 times larger flocculation rate of $R_{f\_Bentonite} = 0.66\ (\text{min}^{-1})$. The mixture of equal amount of Kaolinite and Bentonite has an intermediate flocculation rate of $R_{f\_mixed} = 0.32\ (\text{min}^{-1})$. Following Engel (2000), we will consider Kaolinite having the lowest cohesion, followed by the mixture of

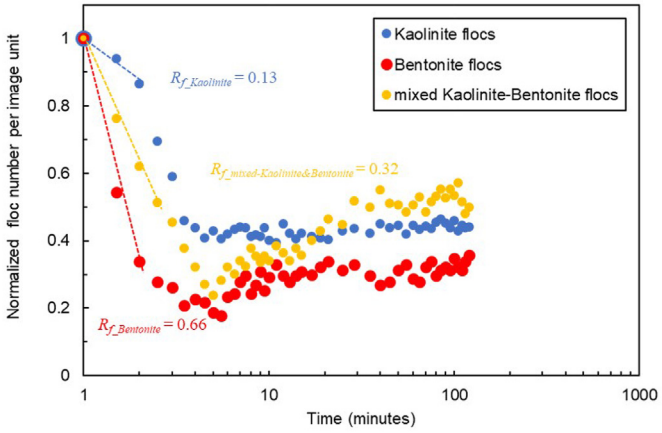

Fig. 3. Temporal (120 min) evolutions of normalized floc number for Kaolinite run (blue, S01), Bentonite run (red, S03) and mixed Kaolinite-Bentonite run (yellow, S05). The initial particle number of each run (S01:1260, S03:782 and S05:1323) is used for normalization. Each data point comes from manually counted floc number from six different images of each pipette sample which covers hundreds to thousands individual flocs.

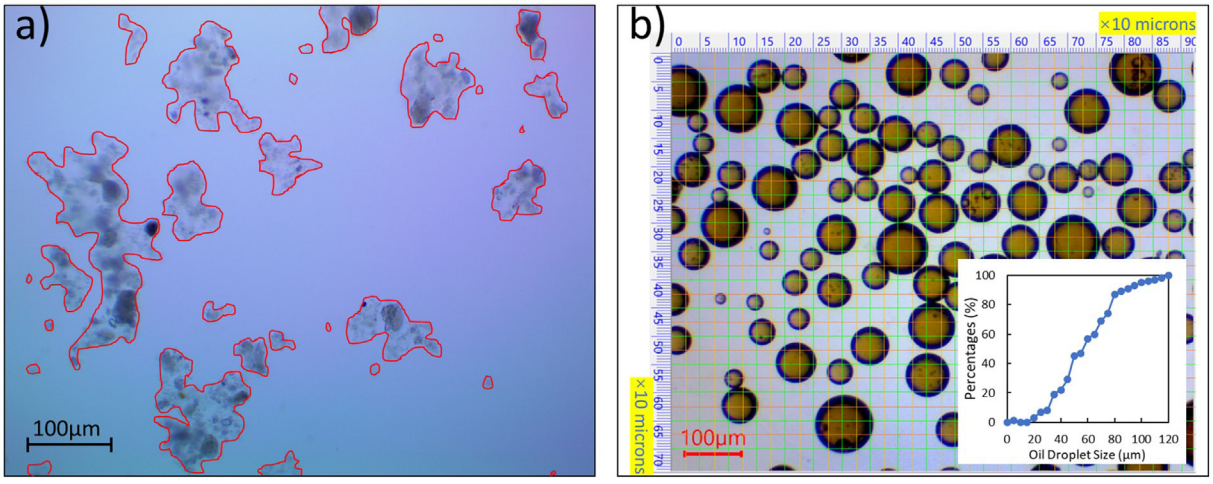

Fig. 2. Examples of digital microscope images. Panel a) shows a snapshot of floc sample from run S03. The red contours indicate the individual floc, which can be recognized manually under the screen by real-time observation. Panel b) shows a snapshot of oil droplets, which can be manually identified and counted to give the averaged droplet size. The oil droplets are formed and measured after 20 min stirring under given turbulence.

Kaolinite-Bentonite and Bentonite is among the most cohesive sediments investigated in this study. This information will be shown later to be very useful for the interpretation of the OMA structure and LabSFLOC-2 settling column experimental results.

We also like to point out that in the Bentonite (red dots) and Kaolinite-Bentonite mixture (yellow dots) samples, normalized floc numbers increase after reaching the maximum flocculation (lowest normalized floc number) at 5∼6 min. The increase is most evident for Kaolinite-Bentonite mixture and consequently the flocs reach an equilibrium stage much later at about 30 min. We believe that this interesting feature is due to the break-up of part of the larger fragile flocs after reaching the maximum flocculation. At the maximum flocculation stage, the participation of more cohesive Bentonite flocs are likely to connect those smaller but denser Kaolinite flocs to form large aggregate structures. However, these large aggregates are fragile and can be further broken into smaller flocs in high turbulence. This complex interaction in mixed Kaolinite-Bentonite sediment can also be seen in the settling column data to be discussed later.

3. Results

3.1. Floc structures

We examine floc structures using high resolution microscope images. Samples from each case presented in Table 1 were collected after the flocculation process reached equilibrium. Fig. 4a$_1$ shows a representative microscope image of pure Kaolinite clay flocs (500 mg·l^{-1}, S01 in Table 1). With the addition of 1 g Texas crude oil (S02 in Table 1), the oil droplets are observed to be attached or embraced within the Kaolinite clay structures (such as Fig. 4a$_{2-4}$). The attachment is limited to the surface of oil droplets while the droplets structure remains intact. The oil-Kaolinite aggregates observed here are consistent with the droplet OMA type reported in the previous studies (Stoffyn-Egli and Lee, 2002; Khelifa et al., 2002), in which oil droplets are coated by sediment aggregates through surface attachment. The quantity of mineral attached to a droplet is highly variable.

The OMA obtained from the Bentonite clay run (S03 in Table 1) are shown in Fig. 4b$_1$. The Bentonite flocs are generally larger than Kaolinite flocs and their size can be up to 100∼200 μm in width and several hundred microns in length. These features are distinct from the pure Kaolinite run (S01) shown in Fig. 4a$_1$. As demonstrated in section 2.2.3 (or Fig. 3), pure Bentonite clay particles are much cohesive and attachable than Kaolinite particles. More importantly, the more cohesive characteristic of Bentonite floc leads to an entirely re-shaped oil-mineral structure (see Fig. 4b$_2$, S04 in Table 1). Compared with oil-Kaolinite flocs, the sphere-shaped oil droplets disappeared. The oil-Bentonite flocs show much larger size of oil soaked mineral having a flake-shaped aggregates up to hundreds of microns in size (see Fig. 4b$_{2-4}$). Compared with the previous studies (Stoffyn-Egli and Lee, 2002; Khelifa et al., 2002; Zhao et al., 2016), the dominant oil-Bentonite aggregates observed here belong to a dense type of oil-aggregate called flake/solid OMA. Flake aggregates have the appearance of membrane structures, which can attain hundreds of microns in length. Their microstructure is highly organized as dendritic or feather-like. Experimental results suggest that high shear strength (i.e. extended or faster agitation) tends to break or crumple flake aggregates. The crumpled flakes (Fig. 4b$_{2-4}$) may be distinguished from mineral-embraced droplet OMA (Fig. 4a$_{2-4}$) by their folds or preferential orientation of the minerals.

After mixing equal amount of Kaolinite and Bentonite clay for Case S05, the mixture flocs contain both Kaolinite floc and

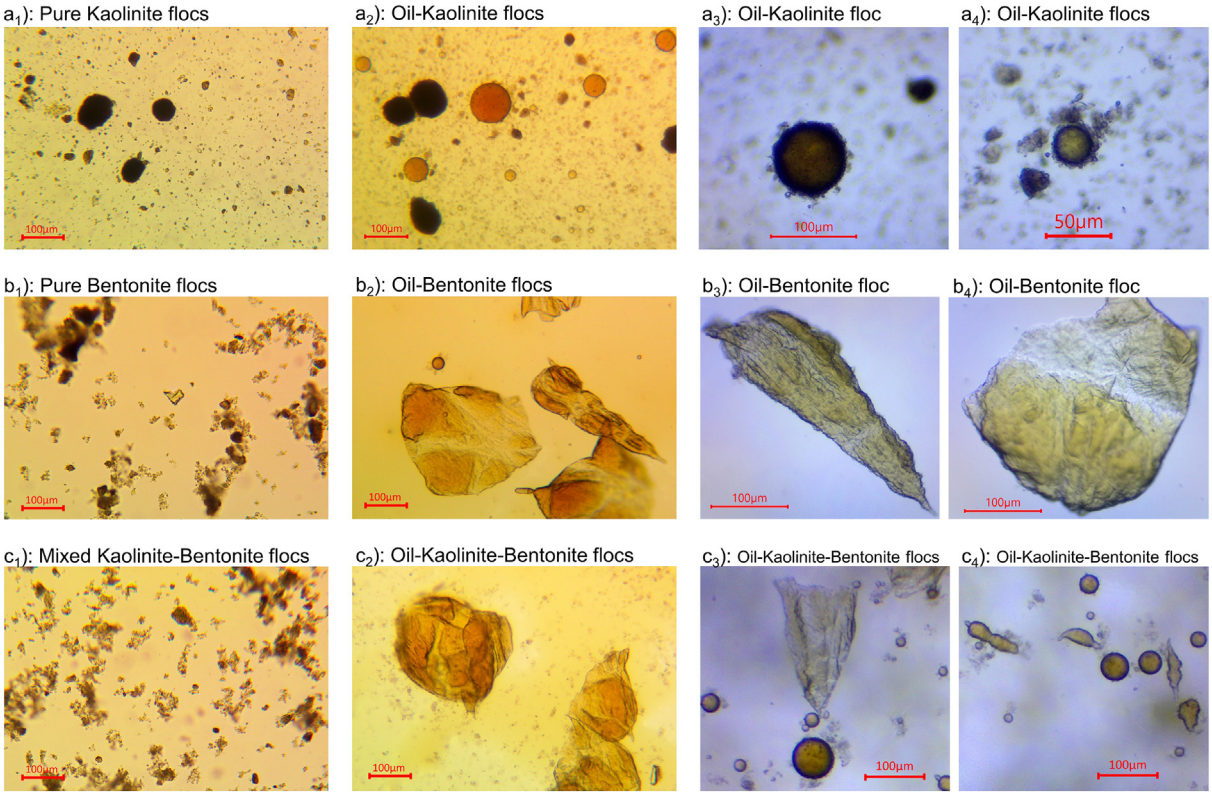

Fig. 4. Floc images from the high-resolution digital microscope camera. a1) Kaolinite (S01) and a2-a4) oil-Kaolinite (S02) samples; b1) Bentonite (S03) and b2-b4) oil-Bentonite (S04) samples; c1) mixed Kaolinite and Bentonite (S05) and c2-c4) oil-Kaolinite-Bentonite (S06) samples.

Bentonite floc structures (see Fig. 4c$_1$), and importantly, although the general size of the mixed flocs (Fig. 4c$_1$) are smaller than pure Bentonite case (Fig. 4b$_1$). The Bentonite floc structure appears to be dominant in the mixture mineral sample. With the addition of oil in the mixture sample S06, large flake shaped OMA can be observed in Fig. 4c$_{2-4}$ which has similar floc size with those in the oil-Bentonite case (S04, see Fig. 4b$_{2-4}$). However, both droplet OMAs and flake OMAs can be observed in Fig. 4c$_{3-4}$.

Because Kaolinite clay has much lower cohesion than Bentonite, the resulting OMA structures are also distinctly different which is expected to lead to different settling velocities. In the next sections, we will investigate different mineral flocs and OMAs settling velocities and discuss their relationship to floc structures.

3.2. Floc physical properties

The previous section provided insights into the floc structures for different types of OMAs by microscopy images. This section is devoted to more quantitative study of floc physical properties, particularly their settling velocities. The scatterplots in Figs. 5a, 6a and 7a illustrate individual spherical-equivalent dry mass weighted floc sizes (x-axis) plotted against their corresponding settling velocities (y-axis) of each sample (see Table 1) collected and analyzed by LabSFLOC-2 camera system. The scatterplots allow subsequent statistical analysis for floc properties using 12 different size classes (size band definition is shown in the bottom of Figs. 5–7). The physical properties shown are the counted floc numbers of each size band (Figs. 5c, 6c and 7c), and the averaged settling velocity (Figs. 5d, 6d and 7d), floc density (Figs. 5e, 6e and 7e), and fractal dimension (Figs. 5f, 6f and 7f) for each size band.

3.3. Kaolinite and Oil-Kaolinite flocs

The scatterplot presented in Fig. 5a indicates that the Kaolinite clay flocs (S01) cover a size range from 20 to 400 μm while their settling velocities vary from 0.04 to 10 mm•s^{-1}. Although with some notable scatters, the floc settling velocities are more or less proportional to floc sizes. Adding oil into Kaolinite mineral (S02) shows negligible change in the floc size range (see Fig. 5b). However, when floc size is greater than about 80 μm, the peak settling velocities (about 4 mm•s^{-1}) show almost no change with respect to floc size. Also, there exist some low-density flocs in the rather large size range of 200∼400 μm with settling velocities ranging from 0.2∼0.6 mm•s^{-1} (around the red constant density line of 16 kg•m^{-3} in Fig. 5b). This is due to the large Oil-Kaolinite flocs having much lower density than those of pure Kaolinite flocs. A more quantitative understanding on these interesting features can be obtained by examining the statistics of 12 size bands.

The number of Kaolinite flocs increases dramatically from Size Band (SB)-1 (20∼40 μm) to SB-3 (80∼120 μm) and then drops quickly from SB-3 to SB-8 (320∼400 μm) (Fig. 5c, blue bands). Since the LabSFLOC-2 analysis can reliably resolve particles size down to 20 μm, it is reminded that some very small flocs are not captured in the results shown here. Adding oil to Kaolinite significantly increases floc number for small size flocs (20∼80 μm) at SB-1 and SB-2 while floc numbers at larger size class are generally lower than or similar to those of pure Kaolinite flocs (Fig. 5c, orange bars). The settling velocities of Kaolinite samples (S01 and S02 in Table 1) averaged for each size class are shown in Fig. 5d. Pure mineral flocs (S01) show a rapid increase of settling velocities with respect to the increase of floc sizes for the entire size class spectrum (SB-1 to SB-8). On the contrary, oil-Kaolinite flocs show milder increase of settling velocity with respect to floc size from SB-1 to SB-6 until a completely different trend is observed for larger size class (SB-6 to SB-8) where the settling velocity decreases as the floc size increases. It is evident that adding oil to Kaolinite decreases settling velocity, particularly for larger floc size classes (by nearly factor 3 in the SB-6 and nearly a factor 7 in the SB-8). Considerable reduction of settling velocity at SB-6 to SB-8 is clearly associated with the significant decrease of floc effective density due to the addition of oil to Kaolinite at this size range (see Fig. 5e). Adding oil reduces floc effective density in all floc size bands but the reduction is much more pronounced at large size class. In SB-2 and SB-3, effective density decreases by approximate 1/3 to 1/4 by adding oil while settling velocity also decreases accordingly. In SB-4 to SB-8, the effective density decreased by half or much more especially in the larger size bands, and their settling velocity shows a remarkable reduction. Since averaged droplet size is about 57 μm (see Fig. 2b), oil participation is more likely to occur in larger size bands. Overall, the results presented here is consistent with the presence of oil as droplets (see Fig. 4a$_2$-a$_4$) having lower density than saltwater or mineral.

The fractal dimension for Kaolinite flocs or Kaolinite-oil flocs is in the range of 2.4∼2.6 except for a small number of large flocs in SB-7/8 (62 and 52 in S01 and S02, respectively, mostly in SB-7). In general, adding oil slightly reduces fractal dimension to 2.4. A notable exception is that when oil is added to Kaolinite, we observed the largest single floc in SB-8 which show a much lower fractal dimension of 2.05 due to containing several low density oil droplets in the large structure.

3.3.1. Bentonite and Oil-Bentonite flocs

In the pure Bentonite sample (S03, Fig. 6a), we observe about 30 very large size flocs up to 400∼700 μm that do not exist in the pure Kaolinite sample (S01). The resulting settling velocity range is also wider (0.01∼20 mm•s^{-1}) than that in Kaolinite samples. A more careful examination further suggests that many large size flocs (in SB-9 SB-12 in Fig. 6c) in pure Bentonite sample (S03) are of very low density (within 50 kg•m^{-3}) and their settling velocities are limited to range of 1∼5 mm•s^{-1}, despite very large floc size. Adding oil further produced a very large floc of 800 μm (Fig. 6b). The upper limit of settling velocity reached to about 10 mm•s^{-1} which is about a factor 2 larger than that of oil-Kaolinite floc (see Fig. 5b).

Comparing to Kaolinite samples (S01 and S02), the most notable difference is that the floc numbers for Bentonite samples are significantly lower. Larger floc sizes and lower floc number in Bentonite samples are consistent with the high flocculation rate (high stickiness) of Bentonite discussed in Section 2.2.3. When oil is added to Bentonite (S04, see Fig. 6d) we observe a monotonic increase of settling velocities with the floc size (except at the largest size class (SB-12), but it only consists of one floc). This trend is different from the oil-Kaolinite sample (S02, Fig. 5d). Moreover, when oil is added to Bentonite, we observe a more rapid increase of settling velocity when floc size increases from SB-9 to SB-12. Comparing to the pure Bentonite condition, we obtain an increase of settling velocity by more than a fact of 2 in SB-11, while recall that for Kaolinite samples, adding oil to Kaolinite (S02) significantly reduces the floc settling velocity. These observations are supported by the floc effective density data. From Fig. 6e, we can see that adding oil to Bentonite clay generally increases floc effective density with the most significant increases occur at SB-1 and SB-9 to SB-12 (contrast with Fig. 5e, adding oil reduces floc effective density in all size bands in Kaolinite samples). This suggests that oil interact differently with Kaolinite and Bentonite samples and it is consistent with their distinct droplet OMA and flake OMA structures presented in Fig. 4. In the Bentonite case (S04), the oil droplets no longer exists and become absorbed into mineral flocs. It is likely that at such micro-scale, oil changes the adhesion characteristic and make the small flocs more compact, dense with lower porosity.

The fractal dimension for Bentonite floc or Bentonite-oil flocs

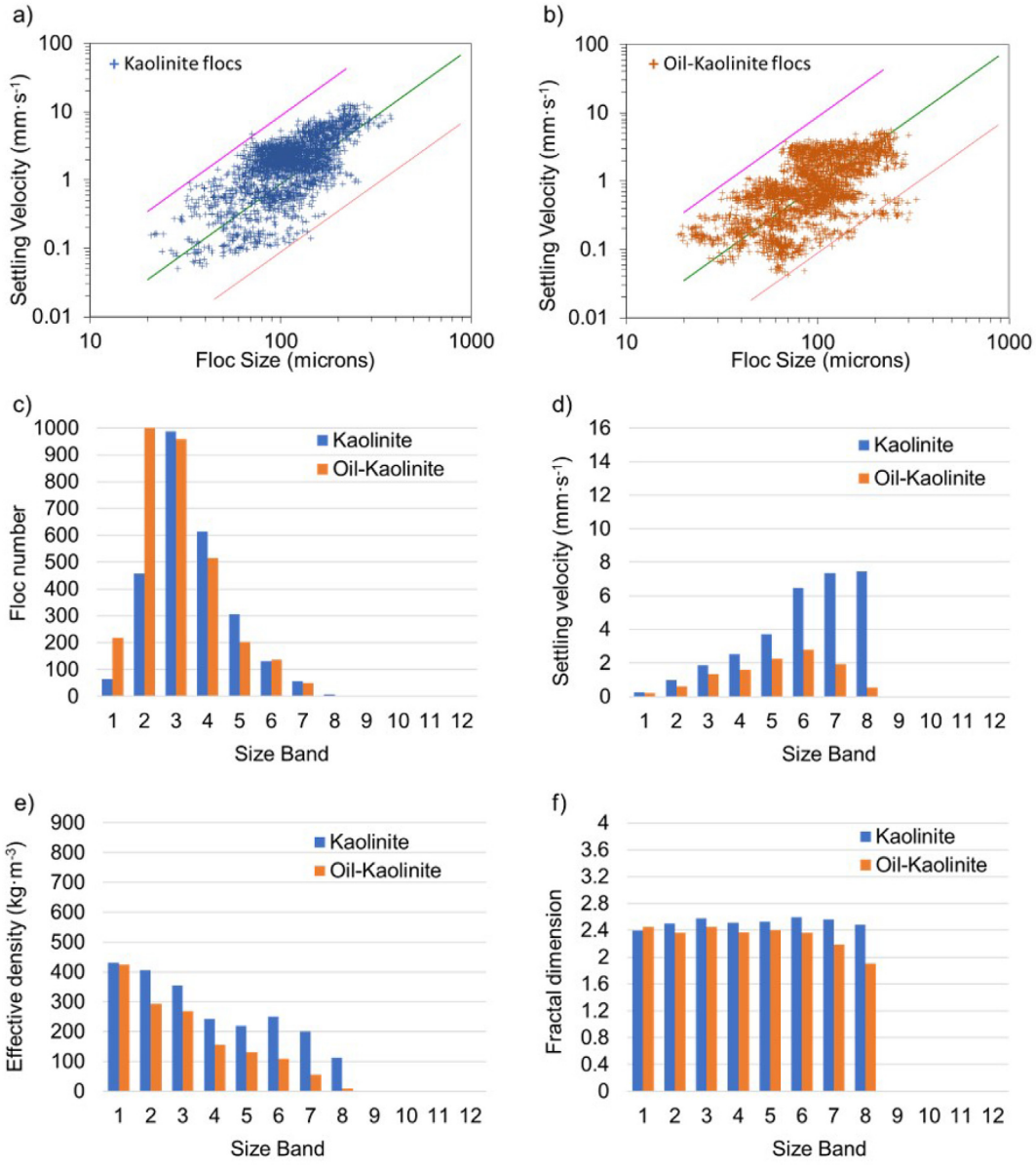

Size Band	1	2	3	4	5	6	7	8	9	10	11	12
Size Range (μm)	20-40	40-80	80-120	120-160	160-200	200-240	240-320	320-400	400-480	480-560	560-640	>640

Fig. 5. Floc characteristics from the LabSFLOC-2 analysis. a) & b) show the plots of floc sizes vs. settling velocities of Kaolinite (S01) and Oil-Kaolinite (S02), respectively. The three diagonal lines represent contours of Stokes settling velocity calculated with a constant effective density of 1,600 kg·m^{-3} (pink line, equivalent to a quartz particle), 160 kg· m^{-3} (green) and 16 kg·m^{-3} (red line). c)-f) show the 12 Size Bands (SB) trends of floc number, settling velocity, floc density and fractal dimensions for Kaolinite (blue) and Oil-Kaolinite (orange) samples. (For interpretation of the references to colour in this figure legend, the reader is referred to the Web version of this article.)

are in the range of 2.2∼2.4 which is slightly lower than those of Kaolinite samples. However, adding oil to Bentonite generally increases fractal dimension with the largest increase occurs at SB-1 with a fractal dimension near 2.5. It is interesting to the point out that, a notable fractal dimension changes after adding oil is in larger size class floc of SB-8 (320∼400 μm) for Kaolinite sample and in the smallest size class of SB-1 (20∼40 μm) for Bentonite sample. This drastic difference is again consistent with different OMA structure of Kaolinite and Bentonite clay.

3.3.2. *Mixed Kaolinite-Bentonite and Oil-Kaolinite-Bentonite flocs*

The settling velocity for mixed Kaolinite-Bentonite flocs (S05) peaks at about 10 mm·s^{-1} for floc size greater than about 100 μm (Fig. 7a). When oil is further added to the mixed Kaolinite-Bentonite sample (Fig. 7b), we observe even higher floc settling velocities exceeding 10 mm·s^{-1}. Generally, both Kaolinite-Bentonite minerals flocs and Oil-Kaolinite-Bentonite flocs show increasing settling velocity with the increasing floc sizes (Fig. 7d) except at the largest size class. In other words, by adding oil to equally mixed Kaolinite and Bentonite mixture, the overall settling velocity trend is similar to that of pure Bentonite (Fig. 6d). This observation can be further confirmed by examining floc effective density shown in Fig. 7e. Similar to adding oil to pure Bentonite (see Fig. 6e), adding oil to Kaolinite-Bentonite mixture generally increase floc effective density and hence the settling velocity also increases in most size bands.

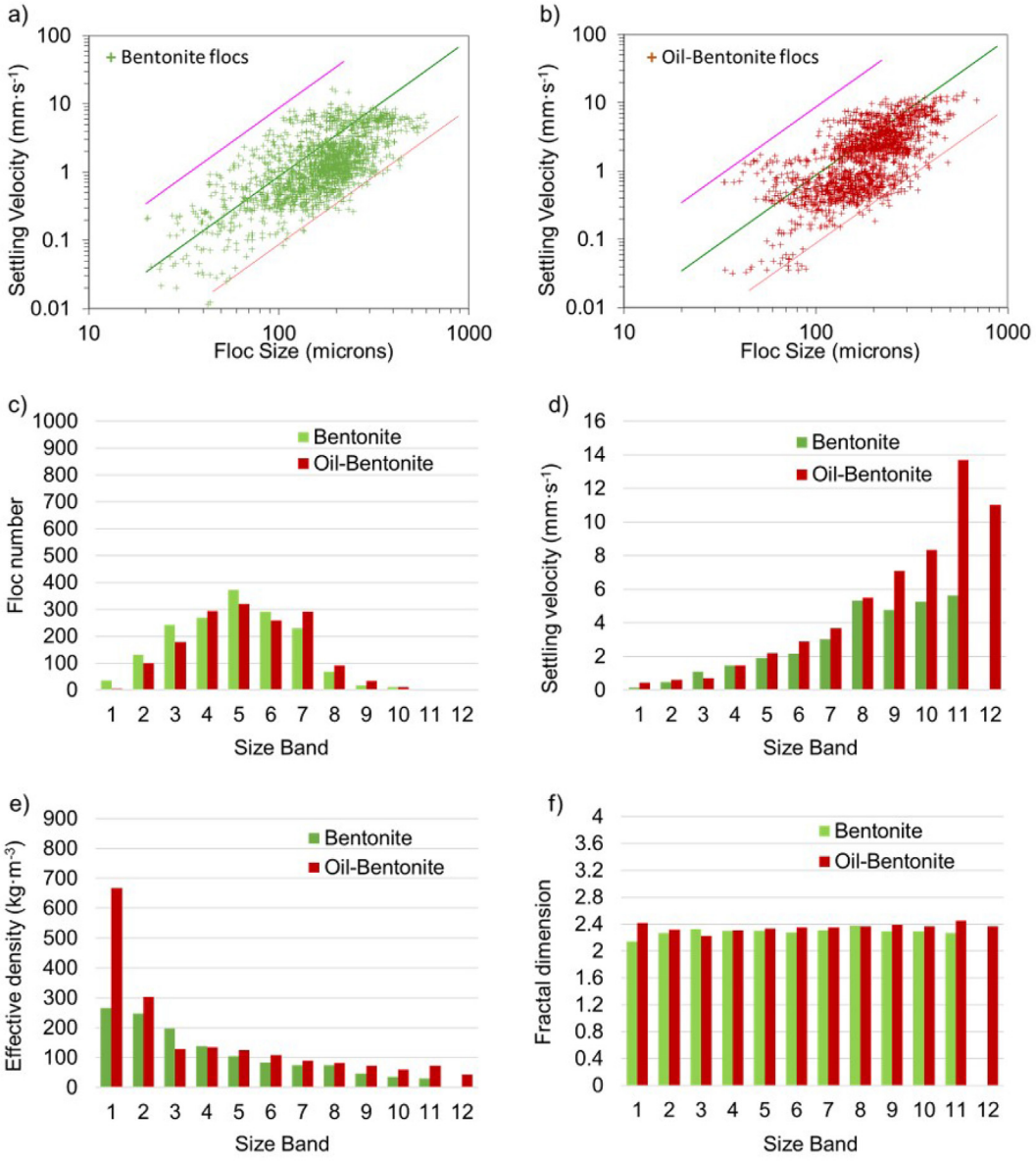

Size Band	1	2	3	4	5	6	7	8	9	10	11	12
Size Range (μm)	20-40	40-80	80-120	120-160	160-200	200-240	240-320	320-400	400-480	480-560	560-640	>640

Fig. 6. Floc characteristics from the LabSFLOC-2 analysis. a) & b) show the plots of floc sizes vs. settling velocities of Bentonite (S03) and Oil-Bentonite (S04), respectively. The three diagonal lines represent contours of Stokes settling velocity calculated with a constant effective density of 1,600 kg·m^{-3} (pink line, equivalent to a quartz particle), 160 kg· m^{-3} (green) and 16 kg·m^{-3} (red line). c)-f) show the 12 Size Bands (SB) trends of floc number, settling velocity, floc density and fractal dimensions for Bentonite (blue) and Oil-Bentonite (orange) samples. (For interpretation of the references to colour in this figure legend, the reader is referred to the Web version of this article.)

There are also some minor but unique differences. In the pure Kaolinite-Bentonite sample, a large number of small sized flocs (<80 μm in SB-1 and SB-2) are observed which are lacking in pure Kaolinite (Fig. 5a) or pure Bentonite (Fig. 6a) samples. This feature can be due to complex interaction of Kaolinte and Bentonite clays having very different stickiness. Firstly, the presence of Kaolinite particles decrease the stickiness of the mixed floc comparing to pure Bentonite condition, which leads to more small flocs comparing to pure Bentonite condition. Moreover, it is likely that the more porous Bentonite flocs, when flocculate with Kaolinite flocs, make the whole mixed flocs more fragile and with the high turbulence level provided, part of the mixture flocs tends to break-up into smaller flocs, even smaller than those in pure Bentonite or Kaolinite cases. Finally, there exist some very small flocs with diameter smaller than 20 μm that cannot be resolved by LabSFLOC-2 system in the Kaolinite cases (see those very small particles resolved by microscope images in Fig. 4a1-a2). When more cohesive Bentonite particles are added and then bonded with Kaolinite particles, these very small flocs may become larger and resolvable by LabSFLOC-2 system. Since these complex processes may require longer interaction time, the feature is consistent with the temporal evolution of normalized floc number shown in Fig. 3 that after the Kaolinte-Bentonite mixture sample reaches maximum flocculation (lowest normalized floc number) at about 5 min, normalized floc number starts to increase and approaches the final equilibrium at about 30 min. Comparing to Bentonite cases, we also observe much

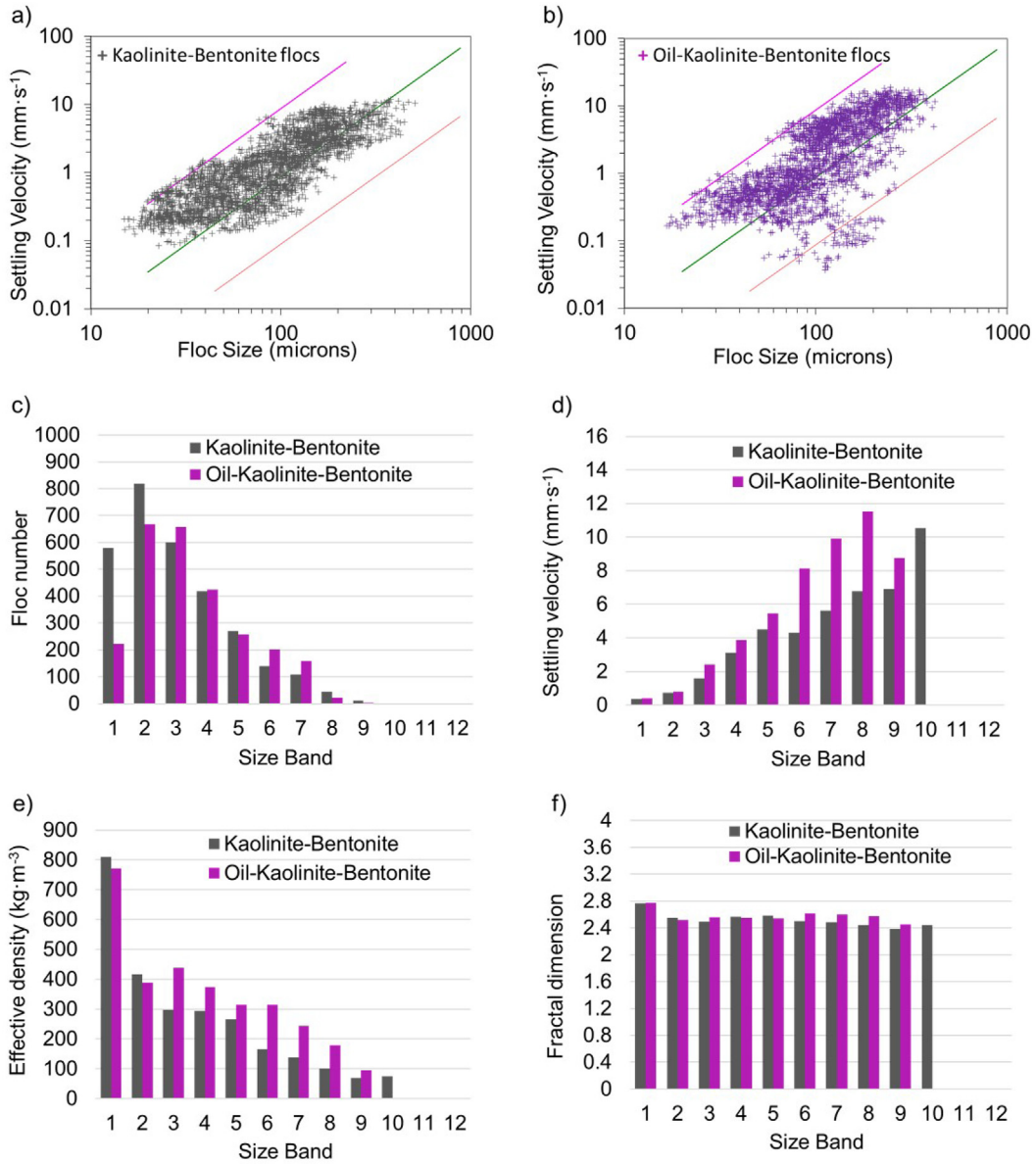

Size Band	1	2	3	4	5	6	7	8	9	10	11	12
Size Range (μm)	20-40	40-80	80-120	120-160	160-200	200-240	240-320	320-400	400-480	480-560	560-640	>640

Fig. 7. Floc characteristics from the LabSFLOC-2 analysis. a) & b) show the plots of floc sizes vs. settling velocities of mixed Kaolinite-Bentonite (S05) and Oil-Kaolinite-Bentonite (S06), respectively. The three diagonal lines represent contours of Stokes settling velocity calculated with a constant effective density of 1,600 kg·m^{-3} (pink line, equivalent to a quartz particle), 160 kg·m^{-3} (green) and 16 kg·m^{-3} (red line). c)-f) show the 12 Size Bands (SB) trends of floc number, settling velocity, floc density and fractal dimensions for mixed Kaolinite-Bentonite (blue) and Oil-Kaolinite-Bentonite (orange) samples. (For interpretation of the references to colour in this figure legend, the reader is referred to the Web version of this article.)

less number of flocs in large size bands (SB-9 to SB-12) in Kaolinite-Bentonite mixture cases and this is clearly due to the presence of less cohesive Kaolinite. Consequently, adding oil to Kaolinite-Bentonite mixture also does not increase the cohesion as much when comparing to adding oil to pure Bentonite. Overall, oil can be considered to preferably interacting with Bentonite and the presence of Kaolinite is of secondary effect to reduce cohesion.

For Kaolinite-Bentonite mixture, the fractal dimension of small sized flocs can be up to 2.8 while the large flocs are of lower value around 2.4 to 2.6. The range of fractal dimension is larger than pure Bentonite (S03) and it is similar to pure Kaolinite (S01) except for the smallest size class (SB-1). By adding oil, flocs fractal dimension in larger size class SB-6 to SB-9 increases and those in small size class SB-1 to SB-5 show negligible change.

3.4. Microflocs and macroflocs

In the cohesive sediment literature, two distinguished floc components: microflocs and Macroflocs, have been utilized to effectively reduce key information provided by the floc spectra (Manning et al., 2010; Manning and Dyer, 2007; Manning and Schoellhamer, 2013). A floc diameter of 160 μm has been often used to distinguish between microflocs and Macroflocs groups (Manning and Dyer, 2002; Manning, 2004; Manning et al., 2010)

and it is also adopted in this study. In order to obtain more general understanding on the floc physical properties, a summary of mean floc properties for the entire floc population and sub-population categorized into microflocs and Macroflocs for all cases are presented in Table 2. Similar to the previous sections, the physical floc properties presented are floc number (N), mean floc diameter ($\overline{D}$), mean effective density ($\overline{\rho_e}$), mean settling velocity ($\overline{W_s}$) and mean fractal dimensions ($\overline{f_n}$).

A comparison between Kaolinite (S01) and Bentonite flocs (S03) show that the Kaolinite flocs in total have around 35 % higher floc number N (2631 versus 1705) and 35 % smaller floc diameter $\overline{D}$ (120 versus 185 μm) (see Table 2). The larger N in Kaolinite is only due to microflocs and in terms of Macrofloc number, Kaolinite has only half of that of Bentonite. The mean effective density $\overline{\rho_e}$ for the entire floc population of Kaolinite floc is about 2.5 times larger than that of Bentonite floc. However, this is particularly due to the Bentonite Macroflocs having significantly low $\overline{\rho_e}$ (only 87 kg• m^{-3}). Our data indicating flocculation in saline water depends on mineral type, particularly for the enhancement of flocculation due to Bentonite, is consistent with several earlier studies (Khelifa et al., 2005b; Zhang et al., 2019). Our study further indicates that despite smaller $\overline{D}$ of Kaolinite flocs, their significantly larger $\overline{\rho_e}$ results in approximately 20 % larger $\overline{W_s}$ than that of Bentonite flocs. Finally, $\overline{f_n}$ of Kaolinite flocs is about 2.54, which is higher than that of Bentonite flocs of around 2.3. The differences of Kaolinite and Bentonite flocs revealed here can be directly attributed to the almost factor 5 higher flocculation rate R_f of Bentonite than Kaolinite in 35 ppt saline water presented in Fig. 3.

By adding oil to the Kaolinite sample (S02 in Table 1), oil-Kaolinite floc number N for the entire population is increased by around 18 % while the corresponding $\overline{D}$ decreases by around 18 %. However, instead of obtaining a slight increase of $\overline{\rho_e}$ commonly expected for decreased cohesion, the $\overline{\rho_e}$ for the entire population also decreases by 20 %. As a result of both reduced $\overline{D}$ and $\overline{\rho_e}$, we obtain a significant reduction of $\overline{W_s}$ by 50 % (decreases from 2.41 mm•s^{-1} to 1.21 mm•s^{-1}, see Table 2). Furthermore, we observe different response of microfloc and Macrofloc fractions due to the addition of oil to Kaolinite in the saline water. The microfloc population shows a 27 % increase in N and 15 % reduction of $\overline{D}$, while the Macrofloc population show 20 % reduced in N and very slight 2.5 % increase (or nearly unchanged) $\overline{D}$. This indicates a minor shift to microfloc population and reduction of cohesion due to the addition of oil. The common trend for both microfloc and Macrofloc is their reduction of $\overline{\rho_e}$: the microflocs show slight (20 %) decrease of $\overline{\rho_e}$ while the Macroflocs show nearly a factor 2 decrease of $\overline{\rho_e}$. As a result, the microfloc and Macrofloc $\overline{W_s}$ are decreased by 43 % and 51 %, respectively. Overall, the participation of lower density oil droplets reduces the OMA density, consistent with the droplet OMA structure presented in Fig. 4. Due to low stickiness of Kaolinite mineral, the direct interaction between oil and Kaolinite is limited to a slight reduction of stickiness and increase of microfloc number. These microflocs tend to attach with the oil droplets (around the surface) forming droplet OMAs with much lower density and settling velocity than the pure Kaolinite mineral flocs.

In terms of the entire floc population, adding oil to Bentonite clay (S04) causes minor change in N, $\overline{D}$ and $\overline{\rho_e}$. However, more significant effect due to oil participation can be identified via a shift between microfloc and Macrofloc populations. We obtain 11 % decrease of microfloc $\overline{\rho_e}$ while the Macrofloc $\overline{\rho_e}$ is increased more significantly by 20% due to the participation of oil. As a result, microfloc $\overline{W_s}$ is nearly unchanged while the Macrofloc $\overline{W_s}$ is increased by 29 %. Since the total flocs are dominated by Macroflocs in the Bentonite cases, the $\overline{W_s}$ for the entire population is increased by 25 % when adding oil.

In the mixed Kaolinite-Bentonite sample (S05), the microfloc $\overline{D}$ is 15 % smaller than that of Kaolinite (S01), and yet in terms of the Macrofloc $\overline{D}$, mixed sample is 13 % larger. In fact, the Macrofloc $\overline{D}$ for mixed Kaolinite-Bentonite sample is nearly comparable (only 5 % smaller) to that of pure Bentonite (S03). Although the $\overline{W_s}$ of mixed Kaolinite-Bentonite sample for the whole floc population (1.97 mm•s^{-1}) appears to be similar to that of pure Bentonite sample (2.0 mm•s^{-1}), the mixed sample reaches the similar $\overline{W_s}$ due to having the largest $\overline{\rho_e}$ (410 kg•m^{-3}) and the smallest $\overline{D}$ (104 μm) comparing to pure Kaolinite (S01) and pure Bentonite (S03) samples. Looking more into the difference, we can see that Macrofloc $\overline{D}$ and $\overline{\rho_e}$ of Kaolinite-Bentonite mixture is about 13 % larger and 12 % smaller than those of pure Kaolinite sample, respectively, which suggests a slight increase of cohesion in Kaolinite-Bentonite flocs due to the presence of Bentonite. On the contrary, in the microfloc population, Kaolinite-Bentonite sample show the smallest and the densest flocs which is similar to the microfloc of pure Kaolinite sample, but distinctly different from those of pure Bentonite sample. The mixed Kaolinite-Bentonite sample possesses a dual feature. Namely, the Kaolinite-like features are observed in microflocs and Bentonite characteristics are more pronounced in Macroflocs.

By adding oil into mixed Kaolinite-Bentonite clay (S06), $\overline{W_s}$ for the entire population increases almost 70 %. However, this increase cannot be explained simply by changes in $\overline{D}$ and $\overline{\rho_e}$. Looking into microfloc and Macrofloc population, adding oil decreases microfloc N by 18 %, increases microfloc $\overline{D}$ by 14 % and reduces $\overline{\rho_e}$ by only 3 %. This slight increase of cohesion cause a 53 % increase of microfloc settling velocity. Oil participation also cause a similar 56 % increase

Table 2
Summary of microfloc and Macrofloc mean quantities of each sample investigated in this study.

Samples	Kaolinite			Bentonite			Kaolinite-Bentonite		
Demarcation	Total	micro	Macro	Total	micro	Macro	Total	micro	Macro
N	2631	2128	503	1705	681	1024	2998	2420	578
$\overline{D}$(μm)	120	101	199	185	105	238	104	76	225
$\overline{\rho_e}$(kg• m^{-3})	315	336	224	127	187	87	410	461	200
$\overline{W_s}$(mm• s^{-1})	2.41	1.82	4.89	2.00	1.08	2.61	1.97	1.27	4.90
$\overline{f_n}$	2.54	2.54	2.55	2.30	2.30	2.30	2.57	2.59	2.53
Samples	Oil-Kaolinite			Oil-Bentonite			Oil-Kaolinite-Bentonite		
Demarcation	Total	micro	Macro	Total	micro	Macro	Total	micro	Macro
N	3102	2696	406	1592	580	1012	2610	1975	635
$\overline{D}$(μm)	102	86	204	198	115	246	120	87	222
$\overline{\rho_e}$(kg• m^{-3})	249	269	113	127	167	104	408	446	290
$\overline{W_s}$(mm• s^{-1})	1.21	1.03	2.41	2.53	1.07	3.36	3.33	1.94	7.63
$\overline{f_n}$	2.40	2.40	2.36	2.33	2.29	2.35	2.57	2.57	2.58

in Macrofloc settling velocity, which is caused by a significant 45 % increase in $\overline{\rho_e}$ with negligible decrease of $\overline{D}$. As a result, $\overline{W_s}$ increases by almost 70 % due to increase of microfloc $\overline{D}$ as well as more dramatic increase of $\overline{\rho_e}$ in Macroflocs.

With the exception of Kaolinite floc and predominant droplet OMAs, generally it is not straightforward to understand the effect of oil on modifying the mineral floc settling velocity without looking into the behavior of floc size classes. Here, we demonstrate that a minimum size class differentiation of microfloc and Macrofloc appears to be useful.

4. Discussion

The results presented in this study indicate the key differences of floccualtion characteristics between Kaolinite and Bentonite OMAs which in respond to their unique OMA structures that are further controlled by mineral stickiness. Kaolinite particles tend to show lower stickiness and the resulting oil-Kaolinite aggregates can be categorized as droplet OMAs. This process is also known as the pickering emulsions (Chevalier and Bolzinger, 2013) (see also Fig. 4a$_2$). The Kaolinite particles/flocs act as a web-structures surrounding the oil droplet preventing its attachment to other oil droplets or further re-bonding to oil slicks. Previous studies (e.g., Zhao et al., 2017) have found that equilibrium OMAs are very stable structure and hardly break. Kaolinite OMAs observed here also consist of more complex multiple mineral flocs. In this case, Kaolinite mineral particles form a much larger structure than individual oil droplet, which is attached or embraced within the larger Kaolinite flocs (Fig. 4a$_{2\text{-}4}$). Because oil droplets structure remains intact, the oil-Kaolinite OMAs show significantly lower effective density and settling velocity than the pure Kaolinite flocs. This finding is consistent with Khelifa et al. (2008) using natural cohesive sediments and suggested that OMAs effective density are 2–3 times lower than pure sediment flocs.

On the other hand, Bentonite particles are of very high stickiness and are observed to form large, fluffy (low density and high porosity) and complex aggregate structure. The large Bentonite aggregates tend to re-shape and absorb or be absorbed by the oil droplets and form denser oil-Bentonite aggregates (Fig. 4b$_{2-4}$). In this case, because the oil droplets no longer exists by themselves and the oil is mainly absorbed at micro-scale level onto the mineral structure, the Bentonite particles can actually become more compact than its pure mineral floc structure (high porosity) and the resulting OMAs are dominated by denser and larger Macroflocs. The overall settling velocities of oil-Bentonite OMAs are also slightly larger than the pure Bentonite flocs. Previous experimental work also indicates that OMAs formed using natural sediment can be as large as 900 μm (O'Laughlin et al., 2017) and their settling velocity can be variable depending on the amount of oil trapped in aggregates (Sun et al., 2010). By adding oil to Kaolinite-Bentonite mixture, oil interacts more actively with Bentonite in Macroflocs to increase the floc effective density and hence settling velocity. However, oil appears to also increase the size of microflocs due to slightly increased cohesion. This study confirms that the stickiness (cohesion) can be one of the key factors in the formation of OMAs. Since chemical dispersant may also affect stickiness during oil-sediment flocculation (Khelifa et al., 2008), the significance of stickiness needs to be investigated more extensively.

The present study apply a rather high turbulence level to generate OMAs. With the measured turbulent dissipation rate of $\varepsilon \approx 0.02\ \mathrm{m^2 \cdot s^{-3}}$, the estimated Kolmogorov length scale $\eta = \left(\frac{\nu^3}{\varepsilon}\right)^{1/4}$ is about 85 μm, which is either slightly smaller (for Kaolinte or Kaolinite-Bentonite cases) or about a factor 2 smaller (for Bentonite cases) than the measured mean floc size. A similar finding that measured OMA size is about a factor 2 or more larger than the estimated Kolmogorov length scale has been reported by (Sun et al., 2010, 2013) for even higher turbulence level than the present study. More extensive investigation on how intense turbulence can limit OMA size can be very useful, especially for modeling purposes.

5. Conclusions

The LabSFLOC-2 system and digital microscopy are utilized to study settling velocities of OMAs and their corresponding floc structures. Consistent with previous studies, droplet OMAs and flake/solid OMAs have been observed. However, we further show that these different OMAs are formed primarily due to the stickiness level of mineral clay and they also lead to different settling velocities. For low stickiness Kaolinite clay, oil participation generates droplet OMAs and the resulting settling velocity is about a factor 2 smaller than the pure Kaolinte flocs. On the other hand, for high stickiness Bentonite clay, oil participation produces flack/solid OMAs and the corresponding settling velocity is slightly larger (about 25 %) than the pure Bentonite flocs. For the mixed Kaolinite-Bentonite OMAs, the resulting settling velocity is about 70 % larger than the pure Kaolinite-Bentonite flocs. While it is clear that the more dominant effect is due to oil interacting with more cohesive Bentonite, the presence of Kaolinite appears to also help increasing the settling velocity by forming denser Kaolinite-Bentonite microflocs. Since the Bentonite clay is one of the most common mineral particles in natural environments, its role in absorbing oil, forming OMAs and influencing the fate of oil need to be incorporated in future modeling efforts.

Declaration of competing interest

The authors declare that they have no known competing financial interests or personal relationships that could have appeared to influence the work reported in this paper.

Acknowledgement

The authors would like to thank James Holyoke for his help and assistance in the laboratory experiments. This research was made possible in part by a grant from the Gulf of Mexico Research Initiative to support CSOMIO (Consortium for Simulation of Oil-Microbial Interactions in the Ocean) (Grant number: SA18-10), and in part by National Science Foundation (OCE-1924532).

References

Ainsworth, C.H., Paris, C.B., Perlin, N., Dornberger, L.N., Patterson III, W.F., Chancellor, E., Murawski, S., Hollander, D., Daly, K., Romero, I.C., 2018. Impacts of the deepwater horizon oil spill evaluated using an end-to-end ecosystem model. PloS One 13 (1), e0190840.

Ajijolaiya, L.O., Hill, P.S., Khelifa, A., Islam, R.M., Lee, K., 2006. Laboratory investigation of the effects of mineral size and concentration on the formation of oil–mineral aggregates. Mar. Pollut. Bull. 52 (8), 920–927.

Almeda, R., Connelly, T.L., Buskey, E.J., 2016. How much crude oil can zooplankton ingest? estimating the quantity of dispersed crude oil defecated by planktonic copepods. Environ. Pollut. 208, 645–654.

Almeda, R., Wambaugh, Z., Wang, Z., Hyatt, C., Liu, Z., Buskey, E.J., 2013. Interactions between zooplankton and crude oil: toxic effects and bioaccumulation of polycyclic aromatic hydrocarbons. PloS One 8 (6), e67212.

Atlas, R.M., Hazen, T.C., 2011. Oil biodegradation and bioremediation: a tale of the two worst spills in us history. Environ. Sci. Technol. 45 (16), 6709–6715.

Benson, T., Manning, A., 2013. Digifloc: the development of semi-automatic software to determine the size and settling velocity of flocs. In: HR Wallingford Report DDY0427-Rt001.

Chanton, J., Zhao, T., Rosenheim, B.E., Joye, S., Bosman, S., Brunner, C., Yeager, K.M., Diercks, A.R., Hollander, D., 2014. Using natural abundance radiocarbon to trace the flux of petrocarbon to the seafloor following the deepwater horizon oil spill. Environ. Sci. Technol. 49 (2), 847–854.

Chevalier, Y., Bolzinger, M.-A., 2013. Emulsions stabilized with solid nanoparticles: pickering emulsions. Colloid. Surface. Physicochem. Eng. Aspect. 439, 23–34.
Crone, T.J., Tolstoy, M., 2010. Magnitude of the 2010 gulf of Mexico oil leak. Science 330 (6004), 634–634.
Daly, K.L., Passow, U., Chanton, J., Hollander, D., 2016. Assessing the impacts of oil-associated marine snow formation and sedimentation during and after the deepwater horizon oil spill. Anthropocene 13, 18–33.
Doshi, B., Sillanpää, M., Kalliola, S., 2018. A review of bio-based materials for oil spill treatment. Water Res. 135, 262–277.
Engel, A., 2000. The role of transparent exopolymer particles (tep) in the increase in apparent particle stickiness (α) during the decline of a diatom bloom. J. Plankton Res. 22 (3), 485–497.
Gratiot, N., Manning, A., 2004. An experimental investigation of floc characteristics in a diffusive turbulent flow. J. Coast Res. 105–113.
Guyomarch, J., Le Floch, S., Merlin, F.-X., 2002. Effect of suspended mineral load, water salinity and oil type on the size of oil–mineral aggregates in the presence of chemical dispersant. Spill Sci. Technol. Bull. 8 (1), 95–100.
Hayakawa, K., Nomura, M., Nakagawa, T., Oguri, S., Kawanishi, T., Toriba, A., Kizu, R., Sakaguchi, T., Tamiya, E., 2006. Damage to and recovery of coastlines polluted with c-heavy oil spilled from the nakhodka. Water Res. 40 (5), 981–989.
Henkel, J.R., Sigel, B.J., Taylor, C.M., 2012. Large-scale impacts of the deepwater horizon oil spill: can local disturbance affect distant ecosystems through migratory shorebirds? Bioscience 62 (7), 676–685.
Hill, P., Khelifa, A., Lee, K., 2002. Time scale for oil droplet stabilization by mineral particles in turbulent suspensions. Spill Sci. Technol. Bull. 8 (1), 73–81.
Huang, C.J., Ma, H., Guo, J., Dai, D., Qiao, F., 2018. Calculation of turbulent dissipation rate with acoustic Doppler velocimeter. Limnol Oceanogr. Methods 16 (5), 265–272.
Jones, A.N., Bridgeman, J., 2016. Investigating the characteristic strength of flocs formed from crude and purified hibiscus extracts in water treatment. Water Res. 103, 21–29.
Khelifa, A., Fingas, M., Brown, C., 2008. Effects of Dispersants on Oil-Spm Aggregation and Fate in Us Coastal Waters. Final Report Grant Number. NA04NOS4190063.
Khelifa, A., Hill, P.S., Lee, K., 2005a. The role of oil-sediment aggregation in dispersion and biodegradation of spilled oil. In: Developments in Earth and Environmental Sciences, vol 3. Elsevier, pp. 131–145.
Khelifa, A., Stoffyn-Egli, P., Hill, P.S., Lee, K., 2002. Characteristics of oil droplets stabilized by mineral particles: effects of oil type and temperature. Spill Sci. Technol. Bull. 8 (1), 19–30.
Khelifa, A., Stoffyn-Egli, P., Hill, P.S., Lee, K., 2005b. Effects of salinity and clay type on oil–mineral aggregation. Mar. Environ. Res. 59 (3), 235–254.
Le Floch, S., Guyomarch, J., Merlin, F.-X., Stoffyn-Egli, P., Dixon, J., Lee, K., 2002. The influence of salinity on oil–mineral aggregate formation. Spill Sci. Technol. Bull. 8 (1), 65–71.
Lee, K., Stoffyn-Egli, P., 2001. Characterization of oil-mineral aggregates. In: International Oil Spill Conference, vol 2001. American Petroleum Institute, pp. 991–996.
Liu, Z., Callies, U., 2019. A Probabilistic Model of Decision Making Regarding the Use of Chemical Dispersants to Combat Oil Spills in the German Bight. Water Research, 115196.
Liu, Z., Liu, J., Zhu, Q., Wu, W., 2012. The weathering of oil after the deepwater horizon oil spill: insights from the chemical composition of the oil from the sea surface, salt marshes and sediments. Environ. Res. Lett. 7 (3), 035302.
Loh, A., Shim, W.J., Ha, S.Y., Yim, U.H., 2014. Oil-suspended particulate matter aggregates: formation mechanism and fate in the marine environment. Ocean Sci. J. 49 (4), 329–341.
Manning, A., 2004. The observed effects of turbulence on estuarine flocculation. Journal of Coastal Research SI 41, 90–104.
Manning, A., Dyer, K., 2007. Mass settling flux of fine sediments in northern european estuaries: measurements and predictions. Mar. Geol. 245 (1–4), 107–122.
Manning, A., Schoellhamer, D., 2013. Factors controlling floc settling velocity along a longitudinal estuarine transect. Mar. Geol. 345, 266–280.
Manning, A.J., Baugh, J.V., Spearman, J.R., Whitehouse, R.J., 2010. Flocculation settling characteristics of mud: sand mixtures. Ocean Dynam. 60 (2), 237–253.
Manning, A.J., Dyer, K.R., 2002. The use of optics for the in situ determination of flocculated mud characteristics. J. Optic. Pure Appl. Optic. 4 (4), S71.
Murawski, S.A., Hogarth, W.T., Peebles, E.B., Barbeiri, L., 2014. Prevalence of external skin lesions and polycyclic aromatic hydrocarbon concentrations in gulf of Mexico fishes, post-deepwater horizon. Trans. Am. Fish. Soc. 143 (4), 1084–1097.
O'Laughlin, C.M., Law, B.A., Zions, V.S., King, T.L., Robinson, B., Wu, Y., 2017. Settling of dilbit-derived oil-mineral aggregates (omas) & transport parameters for oil spill modelling. Mar. Pollut. Bull. 124 (1), 292–302.
Omotoso, O.E., Munoz, V.A., Mikula, R.J., 2002. Mechanisms of crude oil–mineral interactions. Spill Sci. Technol. Bull. 8 (1), 45–54.
Oseen, C., 1927. Neuere methoden und ergebnisse in der hydrodynamik, akad. Verlagsgesellschaft, Leipzig.
Passow, U., 2002. Transparent exopolymer particles (tep) in aquatic environments. Prog. Oceanogr. 55 (3–4), 287–333.
Passow, U., Hetland, R.D., 2016. What happened to all of the oil? Oceanography 29 (3), 88–95.
Passow, U., Ziervogel, K., Asper, V., Diercks, A., 2012. Marine snow formation in the aftermath of the deepwater horizon oil spill in the gulf of Mexico. Environ. Res. Lett. 7 (3), 035301.
Peterson, C.H., Rice, S.D., Short, J.W., Esler, D., Bodkin, J.L., Ballachey, B.E., Irons, D.B., 2003. Long-term ecosystem response to the exxon valdez oil spill. Science 302 (5653), 2082–2086.
Reddy, C.M., Arey, J.S., Seewald, J.S., Sylva, S.P., Lemkau, K.L., Nelson, R.K., Carmichael, C.A., McIntyre, C.P., Fenwick, J., Ventura, G.T., 2012. Composition and fate of gas and oil released to the water column during the deepwater horizon oil spill. Proc. Natl. Acad. Sci. Unit. States Am. 109 (50), 20229–20234.
Reddy, C.M., Eglinton, T.I., Hounshell, A., White, H.K., Xu, L., Gaines, R.B., Frysinger, G.S., 2002. The west falmouth oil spill after thirty years: the persistence of petroleum hydrocarbons in marsh sediments. Environ. Sci. Technol. 36 (22), 4754–4760.
Romero, I.C., Toro-Farmer, G., Diercks, A.-R., Schwing, P., Muller-Karger, F., Murawski, S., Hollander, D.J., 2017. Large-scale deposition of weathered oil in the gulf of Mexico following a deep-water oil spill. Environ. Pollut. 228, 179–189.
Shen, X., Lee, B.J., Fettweis, M., Toorman, E.A., 2018. A tri-modal flocculation model coupled with telemac for estuarine muds both in the laboratory and in the field. Water Res. 145, 473–486.
Sterling Jr., M.C., Bonner, J.S., Ernest, A.N., Page, C.A., Autenrieth, R.L., 2005. Application of fractal flocculation and vertical transport model to aquatic sol–sediment systems. Water Res. 39 (9), 1818–1830.
Stoffyn-Egli, P., Lee, K., 2002. Formation and characterization of oil–mineral aggregates. Spill Sci. Technol. Bull. 8 (1), 31–44.
Stokes, G.G., 1851. On the Effect of the Internal Friction of Fluids on the Motion of Pendulums, vol 9. Pitt Press, Cambridge.
Strom, K., Keyvani, A., 2016. Flocculation in a decaying shear field and its implications for mud removal in near-field river mouth discharges. J. Geophys. Res.: Oceans 121 (4), 2142–2162.
Sun, J., Khelifa, A., Zheng, X., Wang, Z., So, L.L., Wong, S., Yang, C., Fieldhouse, B., 2010. A laboratory study on the kinetics of the formation of oil-suspended particulate matter aggregates using the nist-1941b sediment. Mar. Pollut. Bull. 60 (10), 1701–1707.
Sun, J., Zhao, D., Zhao, C., Liu, F., Zheng, X., 2013. Investigation of the kinetics of oil–suspended particulate matter aggregation. Mar. Pollut. Bull. 76 (1–2), 250–257.
Uncles, R., Mitchell, S., 2017. Estuarine and Coastal Hydrography and Sediment Transport. Cambridge University Press.
Voulgaris, G., Trowbridge, J.H., 1998. Evaluation of the acoustic Doppler velocimeter (adv) for turbulence measurements. J. Atmos. Ocean. Technol. 15 (1), 272–289.
White, H.K., Hsing, P.-Y., Cho, W., Shank, T.M., Cordes, E.E., Quattrini, A.M., Nelson, R.K., Camilli, R., Demopoulos, A.W., German, C.R., 2012. Impact of the deepwater horizon oil spill on a deep-water coral community in the gulf of Mexico. Proc. Natl. Acad. Sci. Unit. States Am. 109 (50), 20303–20308.
Winterwerp, J.C., Van Kesteren, W.G., 2004. Introduction to the Physics of Cohesive Sediment Dynamics in the Marine Environment, vol 56. Elsevier.
Yan, B., Passow, U., Chanton, J.P., Nöthig, E.-M., Asper, V., Sweet, J., Pitiranggon, M., Diercks, A., Pak, D., 2016. Sustained deposition of contaminants from the deepwater horizon spill. Proc. Natl. Acad. Sci. Unit. States Am. 113 (24), E3332–E3340.
Zhang, T., Deng, Y., Cui, Y., Lan, H., Zhang, F., Zhang, H., 2019. Porewater salinity effect on flocculation and desiccation cracking behaviour of kaolin and bentonite considering working condition. Eng. Geol. 251, 11–23.
Zhao, L., Boufadel, M.C., Geng, X., Lee, K., King, T., Robinson, B., Fitzpatrick, F., 2016. A-drop: a predictive model for the formation of oil particle aggregates (opas). Mar. Pollut. Bull. 106 (1–2), 245–259.
Zhao, L., Boufadel, M.C., King, T., Robinson, B., Gao, F., Socolofsky, S.A., Lee, K., 2017. Droplet and bubble formation of combined oil and gas releases in subsea blowouts. Mar. Pollut. Bull. 120 (1–2), 203–216.
Zhao, L., Torlapati, J., Boufadel, M.C., King, T., Robinson, B., Lee, K., 2014. Vdrop: a comprehensive model for droplet formation of oils and gases in liquids-incorporation of the interfacial tension and droplet viscosity. Chem. Eng. J. 253, 93–106.